Journal of Applied Electrochemistry **29**: 1351–1354, 1999.

Short communication

Spinel-type oxides $LiMn_{2-x}M_xO_4$ [M=Co, Fe, (CoFe)] as electrocatalyst for oxygen evolution/reduction in alkaline solution

N. LI*, X. YAN, Y. JIN, S. LI and B. LIN
Institute of Physical Chemistry, Peking University, Beijing, 100871, China
*(*author for correspondence)*

Received 10 September 1998; accepted in revised form 8 March 1999

Key words: electrocatalysts, oxygen evolution/reduction, spinel oxides

1. Introduction

The secondary metal–air battery is an attractive power source due to its high specific energy [1], but it is not used widely because there is a lack of an ideal electrocatalyst for the bifunctional air electrode. Such an electrocatalyst must possess high activity, low price and be stable in alkaline solution [2, 3]. Basically, electrocatalysts with large specific surface areas are necessary to obtain high activity [3–5]. Some spinel-type oxides [6–8] show promise as good electrocatalysts for the bifunctional air electrode because of their high activity for oxygen evolution in alkaline solution. Spinel-type oxides $LiMn_{2-x}M_xO_4$ (M = 3d metal) have been examined as cathode materials for lithium batteries and rechargeable lithium ion batteries [9–12]. In a previous paper [13], we reported that $LiMn_{2-x}Co_xO_4$ ($x = 1.0$, 1.2, 1.4, 1.6) showed good electrocatalytic activity in 7 M KOH solution. In this study, three series of spinel-type complex oxides $LiMn_{2-x}Co_xO_4$ (A series, $x = 0$, 0.2, 0.4, 0.6, 0.8) $LiMn_{2-x}Fe_xO_4$ (B series, $x = 0.2$, 0.4, 0.6, 0.8) and $LiMn_{2-x}Co_{x/2}Fe_{x/2}O_4$ (C series, $x = 0.2$, 0.4, 0.6, 0.8) have been synthesized by an improved amorphous citric precursor method (IACP), and their electrocatalytic performance has been evaluated in gas-diffusion oxygen electrodes.

2. Experimental details

2.1. *Catalyst preparation and characterization*

Three series of spinel-type complex oxides $LiMn_{2-x}Co_xO_4$, $LiMn_{2-x}Fe_xO_4$ and $LiMn_{2-x}Co_{x/2}Fe_{x/2}O_4$ were synthesized by the IACP method. The solutions of nitrates of constituent ions and citric acid were mixed, and then a certain amount of carbon black (Cabot VXC-72) with a overall surface area of 254 $m^2\ g^{-1}$ was added to prevent agglomeration of the particles of the oxides [13]. The mixture was decomposed at 200 °C for 1 h, then A series samples were calcined at 360 °C, B and C series samples were calcined at 370 °C in air for 4 h, then cooled with furnace. The amount of carbon impurities after calcination of the compounds were no more than 0.52, 0.25 and 0.29 (wt %) for A, B and C series oxides, respectively (Elementar Vario EL). The specific surface areas of the oxides were measured by the Brunauer–Emmet–Teller (BET) method (N_2 adsorption). The lattice parameters and average grain size were examined by powder X-ray diffraction (Rigaku D/max-rA, CuK_α, 40 kV, 150 mA). A graphite diffracted beam monochrometer was used to improve signal-to-noise characteristics. The constant k_m of H_2O_2 decomposition reaction catalysed by the oxides was measured in 7 M KOH at 20 °C (error is less than 10%) [3, 4, 6].

2.2. *Electrode preparation and electrochemical measurement*

The gas-diffusion electrodes were composed of a gas-diffusion layer and a reaction layer. The gas-diffusion layer consisted of ethyne black (70 wt %), PTFE (30 wt %) and an embedded nickel mesh (80 mesh, current-collector). The reaction layer consisted of 25 wt % oxide catalyst (1.5 mg cm^{-2}), 60 wt % carbon black and 15 wt % PTFE. These layers were prepared by using the procedure similar to that of Shimizu et al. [3]. Ethyne black or a carbon-oxide catalyst mixture was suspended in water containing a dispersant (triton X-100 : water = 1 : 500). After the PTFE dispersion was added and mixed, the suspension was evaporated and dried for 2 h at 100 °C. The dried products were heated for 3 h in N_2 at 300 °C for the gas-diffusion layer and at 280 °C for the reaction layer respectively. The obtained cakes were pulverized into fine powders. The powders were cool-pressed onto the Ni mesh to make a stacking of the layers. Then the assembly was sintered for 15 min at 350 °C, and hot-pressed into a laminated sheet, 18 mm in diameter and about 0.4 mm thick, under 6 MPa for 20 s. The half cell was developed by Li et al. [14]. The polarization curves, referred to a Hg/HgO electrode, were measured in 7 M KOH at 21 °C under oxygen flow (100 $cm^3\ min^{-1}$).

3. Results and discussion

Powder X-ray diffraction (XRD) analysis was performed for all the samples. The typical XRD patterns are given in Figure 1. Spinel-type complex oxides were obtained for each x value in the A, B and C series. The samples (with $x = 0$, 0.2) are more or less accompanied by a small quantity of impure phase Mn_2O_3 (JCPDS, 41–1442), as seen in Figure 1.

The cubic lattice parameters a, average grain size $D_{(100)}$ and specific surface areas S of the IACP oxides, together with their respective H_2O_2 decomposition constants $k_s(= k_m/S)$ are shown in Tables 1–3. The lattice parameters a of the A and C series decreased with x. The variation of the parameters with x for the B series is very small. These results are very similar to the results reported by Tarascon et al. [9]. The oxide $LiMn_2O_4$, with $a < 0.8245$ nm, should be considered as non-stoichiometric lithium manganospinel [15, 16]. The average grain size for all the samples is in the nanoscale. The addition of carbon black weakened the agglomerates of the oxide particles and increased the surface area. In Tables 1–3 the constants, k_s, of the H_2O_2 decomposition reaction normalized to specific surface area are also shown. The high k_s values imply that A, B and C series oxides are very effective in decreasing H_2O_2 concentration.

Figures 2–7 show cathodic and anodic polarization curves of A, B and C series oxides, respectively. The curves were recorded under oxygen flow for a pure VXC-72 carbon electrode (no catalyst) and a bifunctional air electrode with 25% $LiMn_{2-x}M_xO_4$ in the catalyst layer. The best current–potential curves (for anodic and cathodic reactions) of A, B and C series oxides are shown in Figure 8. The electrodes loaded with the catalysts performed much better than the pure carbon electrode. The k_s value (Tables 1–3) can be related to the oxygen reduction reaction. As reported in the literature [17, 18], on high surface-area carbon, oxygen is mainly reduced in a two-electron reaction to form H_2O_2. The $LiMn_{2-x}M_xO_4$ functions as catalyst and leads to more rapid decomposition of H_2O_2 and a subsequent decrease in overpotential for oxygen reduction. The electrode loaded with $LiMn_{1.4}Co_{0.6}O_4$ was found to show high performance for oxygen reduction, its current density being as high as -2500 mA cm^{-2} at -300 mV vs Hg/HgO in 7 M KOH at 21 °C. $LiMn_{1.4}Co_{0.6}O_4$ seems to be the best catalyst for decomposition of H_2O_2 among A, B and C series oxides under the experimental conditions used. For oxygen evolution, the $LiMn_{2-x}M_xO_4$ functions as electrocatalyst and reduces the overpotential. The oxygen evolution mechanism on the oxides is not clear. The electrode loaded with $LiMn_{1.6}Co_{0.4}O_4$, which was found to be very active for oxygen reduction, also showed high activity for oxygen evolution. The high activity of $LiMn_{2-x}M_xO_4$ ($x > 0.2$) as catalyst for decomposition of H_2O_2 appears to be associated with the high activity for oxygen evolution. One remarkable

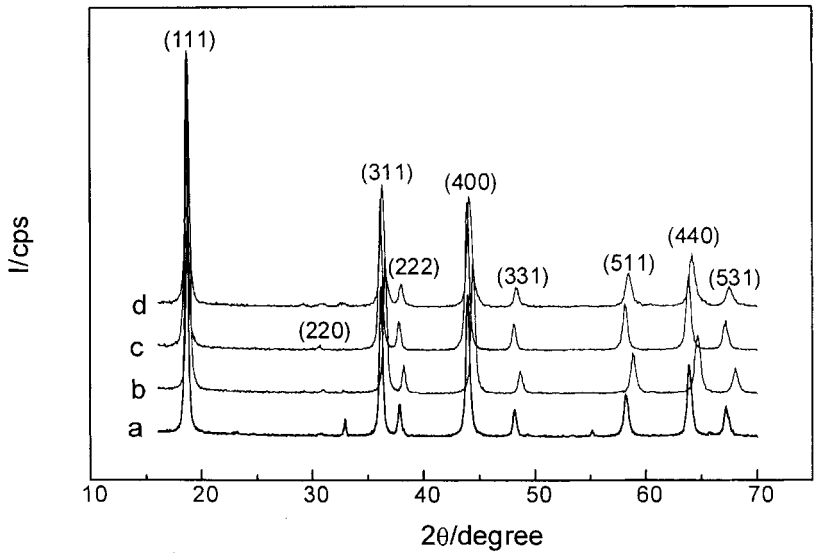

Fig. 1. Powder X-ray diffraction patterns of the samples $LiMn_{2-x}M_xO_4$: (a) M=Mn, $x = 0$, (b) M=Co, $x = 0.4$, (c) M=Fe, $x = 0.4$, (d) M=$Fe_{0.5}Co_{0.5}$, $x = 0.4$.

Table 1. Lattice parameter (a), average grain size ($D_{(100)}$) and specific surface area (S) of the improved amorphous citric precursor (IACP) oxides, together with their respective H_2O_2 decomposition constants (k_s) for A series samples

x in $LiMn_{2-x}Co_xO_4$	$x = 0$	$x = 0.2$	$x = 0.4$	$x = 0.6$	$x = 0.8$
a/nm	0.8226	0.8183	0.8135	0.8109	0.8074
$D_{(100)}$/nm	22	25	23	21	16
S/m^2 g^{-1}	17.8	21.0	25.2	30.7	42.3
k_s/10^{-1} s^{-1} m^{-2}	1.67	3.00	2.13	1.33	0.66

Table 2. Lattice parameter (a), average grain size ($D_{(100)}$) and specific surface area (S) of the improved amorphous citric precursor (IACP) oxides, together with their respective H_2O_2 decomposition constants (k_s) for B series samples

x in $LiMn_{2-x}Fe_xO_4$	$x = 0.2$	$x = 0.4$	$x = 0.6$	$x = 0.8$
a/nm	0.8221	0.8235	0.8237	0.8243
$D_{(100)}$/nm	25	25	31	34
$S/m^2\,g^{-1}$	23.4	18.5	31.4	41.6
$k_s/10^{-1}\,s^{-1}\,m^{-2}$	1.70	1.87	0.60	0.41

Table 3. Lattice parameter (a), average grain size ($D_{(100)}$) and specific surface area (S) of the improved amorphous citric precursor (IACP) oxides, together with their respective H_2O_2 decomposition constants (k_s) for C series samples

$LiMn_{2-x}Co_{x/2}Fe_{x/2}O_4$	$x = 0.2$	$x = 0.4$	$x = 0.6$	$x = 0.8$
a/nm	0.8208	0.8206	0.8183	0.8163
$D_{(100)}$/nm	27	19	20	15
$S/m^2\,g^{-1}$	19.3	27.0	26.4	27.9
$k_s/10^{-1}\,s^{-1}\,m^{-2}$	4.02	2.55	2.11	1.18

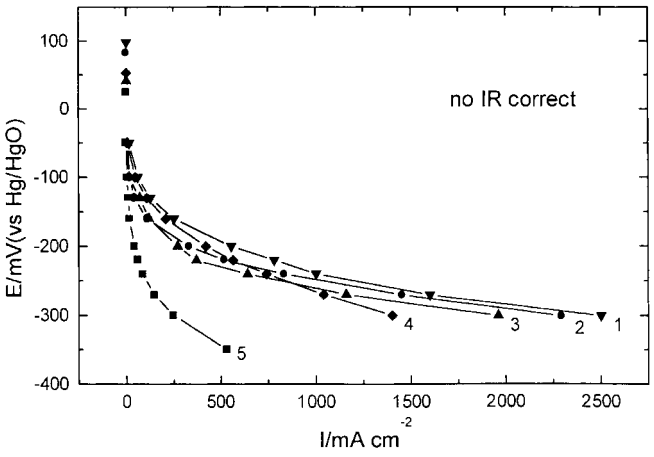

Fig. 2. Cathodic polarization curves (for oxygen reduction) of gas-diffusion carbon electrodes loaded with $LiMn_{2-x}Co_xO_4$ with different x values: (1) $x = 0.6$, (2) $x = 0$, (3) $x = 0.2$, (4) $x = 0.8$, (5) carbon only.

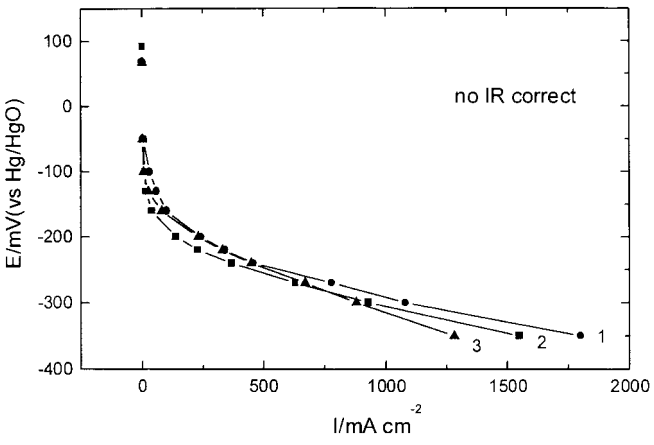

Fig. 3. Cathodic polarization curves (for oxygen reduction) of gas-diffusion carbon electrodes loaded with $LiMn_{2-x}Fe_xO_4$ with different x values: (1) $x = 0.6$, (2) $x = 0.2$, (3) $x = 0.8$.

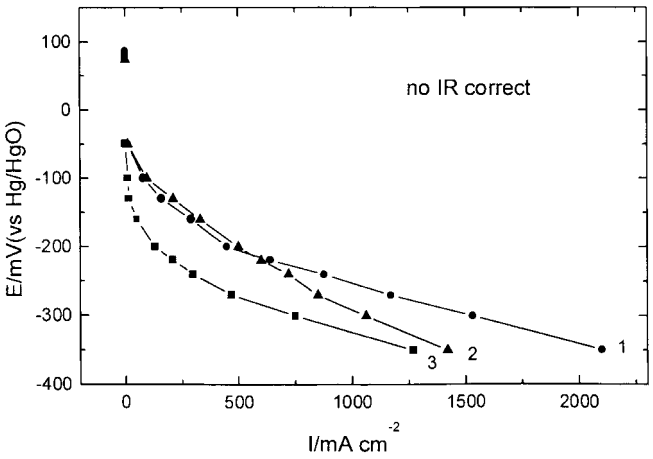

Fig. 4. Cathodic polarization curves (for oxygen reduction) of gas-diffusion carbon electrodes loaded with $LiMn_{2-x}Co_{x/2}Fe_{x/2}O_4$ with different x values: (1) $x = 0.6$, (2) $x = 0.8$, (3) $x = 0.2$.

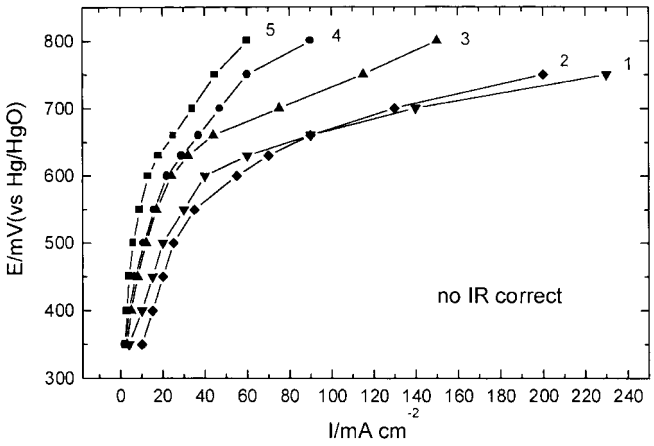

Fig. 5. Anodic polarization curves (for oxygen evolution) of gas-diffusion carbon electrodes loaded with $LiMn_{2-x}Co_xO_4$ with different x values: (1) $x = 0.6$, (2) $x = 0.8$, (3) $x = 0.2$, (4) $x = 0$, (5) carbon only.

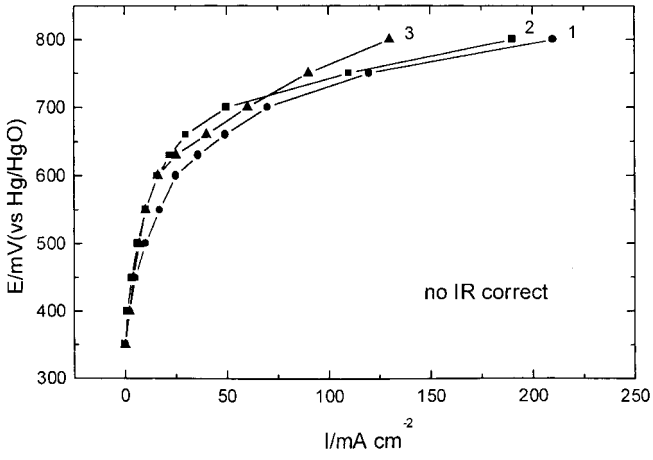

Fig. 6. Anodic polarization curves (for oxygen evolution) of gas-diffusion carbon electrodes loaded with $LiMn_{2-x}Fe_xO_4$ with different x values: (1) $x = 0.6$, (2) $x = 0.2$, (3) $x = 0.8$.

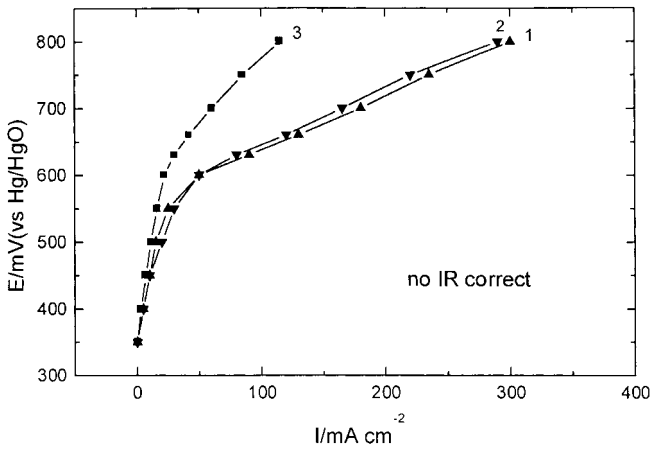

Fig. 7. Anodic polarization curves (for oxygen evolution) of gas-diffusion carbon electrodes loaded with $LiMn_{2-x}Co_{x/2}Fe_{x/2}O_4$ with different x values: (1) $x = 0.6$, (2) $x = 0.8$, (3) $x = 0.2$.

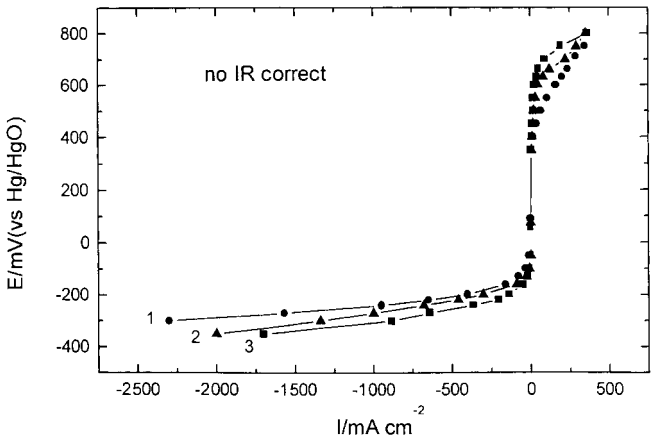

Fig. 8. Cathodic and anodic polarization curves of gas-diffusion carbon electrodes: (1) loaded with 25% $LiMn_{1.6}Co_{0.4}O_4$, (2) loaded with 25% $LiMn_{1.6}Co_{0.2}Fe_{0.2}O_4$, (3) loaded with 25% $LiMn_{1.6}Fe_{0.4}O_4$.

result was found for $LiMn_{1.6}Co_{0.4}O_4$ especially for the oxygen evolution reaction, as shown in Figure 8. The potential difference at 100 mA cm^{-2} between the oxygen evolution and reduction reaction is less than 700 mV when using this catalyst. For a rechargeable metal–air battery the energy efficiency at 100 mA cm^{-2} could be in the range 60–70%.

4. Conclusion

The IACP method weakened the agglomerates of the oxide particles and increased the specific surface area. As a result, the spinel-type oxides (especially for $LiMn_{1.6}Co_{0.4}O_4$) showed high electrochemical activity for oxygen evolution and reduction. With the compounds described in this paper, it should be possible to increase the energy efficiency of the zinc–air system by about 10%.

References

1. M.H. Frank and J.S. Mark, Proc. of the 9th Annu. Battery Conf. Appl. Adv., January 11–13 (1994).
2. L. Swetter and J. Giner, *J. Power Sources* **22** (1988) 399.
3. Y. Shimizu, K. Uemura, H. Matsuda, N. Miura and N. Yamazoe, *J. Electrochem. Soc.* **137** (1990) 3430.
4. H.M. Cota, T. Katan, M. Chin and F.J. Schoenweis, *Nature* **4951** (1964) 1281.
5. S.K. Tiwari, S.P. Singh and R.N. Singh, *J. Electrochem. Soc.* **143** (1996) 1505.
6. J.R. Goldstein and A.C.C. Tseung, *J. Catal.* **32** (1974) 452.
7. R.N. Singh, J.-F. Koening, G. Poillerat and P. Chartier, *J. Electrochem. Soc.* **137** (1990) 1408.
8. B. Marsan, N. Fradette and G. Beandoin, *J. Electrochem. Soc.* **139** (1992) 1889.
9. J.M. Tarascon, E. Wang, F.K. Shokoohi, W.R. Mckinnon and S. Colson, *J. Electrochem. Soc.* **138** (1995) 2859.
10. R. Bittihn, R. Herr and D. Hoge, *J. Power Sources* **43–44** (1993) 223.
11. G. Li, H. Ikuta, T. Uchida and M. Wakihara, *J. Electrochem. Soc.* **143** (1996) 178.
12. K. Amine, H. Tukamoto, H. Yasuda and Y. Fujita, *J. Electrochem. Soc.* **143** (1996) 1607.
13. N. Li, X. Yan, W. Zhang and B. Lin, *J. Power Sources* **74** (2) (1998) 255.
14. Q. Li, G. Xiao, H.A. Hjuler, R.W. Berg and N. J. Bjerrum, *J. Electrochem. Soc.* **141** (1994) 3114.
15. M.H. Rossouw, A. de Kock, L.A. de Picciotto, M.M. Thackeray, W.I.F. David and R.M. Ibberson, *Mat. Res. Bull.* **25** (1990) 173.
16. C. Masquelier, M. Tabuchi, K. Ado, R. Kanno, Y. Kobayashi, Y. Maki, O. Nakamura and J.B. Goodenough, *J. Solid State Chem.* **123** (1996) 255.
17. H. Falcon and R.E. Carbonio, *J. Electroanal. Chem.* **69** (1992) 339.
18. S. Mueller, K. Striebel and O. Haas, *Electrochim. Acta* **39** (1994) 1661.